Article

Using Remote Sensing Techniques to Assess Land-Cover Change and Degradation in the Deserts of the Southeast Iberian Peninsula

Emilio Ramírez-Juidias [1]*, Antonio Madueño-Luna [2], José Miguel Madueño-Luna [3], Miguel Calixto López-Gordillo [3] and Jorge Luis Leiva-Piedra [4]

[1] Instituto Universitario de Arquitectura y Ciencias de la Construcción (IUACC), Universidad de Sevilla, 2 Reina Mercedes Avenue, 41012 Seville, Spain
[2] Departamento de Ingeniería Aeroespacial y Mecánica de Fluidos, Universidad de Sevilla, 41092 Seville, Spain
[3] Departamento de Ingeniería Gráfica, Universidad de Sevilla, 41092 Seville, Spain
[4] Laboratorio de Investigación en Teledetección, Universidad Tecnológica del Perú, Intersección Avenida El Progreso s/n-Vía de Evitamiento, Chiclayo 14001, Peru
* Correspondence: erjuidias@us.es

Abstract: Many drylands around the world have seen both soil and vegetation degradation around watering points. It can be seen in spaceborne imagery as radial brightness belts that fade with distance from the water areas. The study's primary goal was to characterize spatio-temporal land degradation/rehabilitation in the drylands of the southeast Iberian Peninsula. The brightness index of Tasseled Cap was discovered to be the best spectral transformation for enhancing the contrast between the bright-degraded areas near the points and the darker surrounding areas far from and in-between these areas. To comprehend the spatial structure present in spaceborne imagery of two desert sites and three key time periods, semi-variograms were created (mid-late 2000s, around 2015, and 2020). In order to assess spatio-temporal land-cover patterns, a geostatistical model (kriging) was used to smooth brightness index values extracted from 30 m spatial resolution images. To assess the direction and intensity of changes between study periods, a change detection analysis based on kriging prediction maps was performed. These findings were linked to the socioeconomic situation prior to and following the EU economic crisis. The study discovered that degradation occurred in some areas as a result of the region's agricultural activities being exploited.

Keywords: Andalusia; remote sensing; desert of Tabernas; Sierra Alhamilla; Almería; mathematical models

1. Introduction

Overgrazing, according to the United Nations Environment Program (UNEP), is the practice of allowing a much greater number of animals to graze at a location than it can actually support. As a result, in terms of plant density, plant chemical content, community structure, and soil erosion, overgrazing by various types of livestock is perhaps the most significant anthropogenic activity that degrades rangelands and causes desertification [1]. Overgrazing degrades approximately 75 million ha of land globally, destroying the original biotic functions [2]. According to [3], Land (soil and vegetation) degradation is particularly associated with areas surrounding natural or artificial water sources, such as wells or boreholes, in arid and semi-arid environments.

During grazing, domestic animals tend to concentrate near watering points, with the concentration gradually decreasing as distance from water increases [4-5]. Typically, grazing occurs about 5 km of the watering point, but this can increase up to 20 km in extreme conditions [3, 6]. It is also interesting to specify that the radial grazing pattern, known as the "piosphere", was named after the Greek root "pios" meaning "drink" [3]. On the other hand, and according to [7], "grazing gradient" refers to the spatial patterns in soil or vegetation resulting from grazing and can indicate land

 doi:10.20944/preprints202306.0781.v1

degradation. For this reason, most of the drylands used for pastoralism show degraded features caused by grazing activities.

Studies conducted using ground measurements and/or analysis of data obtained from remote sources have been conducted to observe the changes in grazing effects on rangelands. A variety of biotic, abiotic, and environmental effects have been documented in the literature, such as those discussed in references [8-11]. Studies have looked at how vegetation cover, species richness and diversity, and the spread of biological soil crusts change depending on the distance from the watering point. Further, research has been conducted on soil chemistry and physical properties, as well as the effect of erosion and trampling. The majority of the ground-based measurements are taken from samples along transects, and these samples are taken from plots of varying sizes, ranging from 1 to 100 m^2. It has been demonstrated that methods which assess only limited areas are heavily influenced by natural changes in vegetation composition and landscape features that cannot be confidently linked to the effects of grazing [12]. Traditional ground-based measurements are laborious, relatively costly, and distant sites are not available for regular repeatable sampling [7]. [4] postulated that grazing effects cannot be monitored when the measurement is conducted in a limited spatial scope. The challenges associated with semi-arid rangelands are exacerbated, yet remote sensing data can be utilized to counter them.

Since the radial pattern around watering points is clearly visible from satellite imagery, recent studies have been conducted by interpreting and modeling the remote sensing data [13, 14], which can be processed in a semi-automated and repeatable manner over large and distant regions. For this reason, different remote-sensing models that utilize geographic information systems techniques have been created to calculate the spatial spread of various elements in the vicinity of watering points [5, 13-15].

Various studies have indicated that the circular pattern of grazing gradients around watering points results in similar patterns for various biotic, abiotic, and environmental variables. Vegetation cover, measured using indices such as SAVI (soil adjusted vegetation index) or NDVI (normalized difference vegetation index) [5, 15-17], annuals production and grass [14, 18], organic content, soil pH and bush encouragement, nitrate and phosphate [11], soil nutrient concentrations [19], and track density [20], are commonly used variables that follow this pattern. The improvement or decline of each variable does not change significantly after a few kilometers from the watering point. However, in some cases, such as inversed, composite, and complex gradients [17, 21], different responses were observed. The composite gradient is associated with non-native species replacing desirable ones, while the inverse gradient is observed in areas with a dam and mostly woody vegetation. The complex gradient is seen in areas where vegetation growth is decreased in runoff and erosion areas, but increased in run-on and sediment deposits. According to [11], the grazing effects form a radial pattern with a sacrifice zone up to 50 m from the borehole, a nutritious grass zone up to 800 m, dominated by palatable and grass species, and a bush encroachment zone up to 2000 m. This distance is considered as the farthest point where grazing has a significant impact.

Intensive grazing near water sources is a global occurrence. However, this research was carried out in the arid regions of Southeast Iberian Peninsula, focusing on the socioeconomic changes that took place in this region towards the end of the 20th century. In these desert areas, livestock farming is a significant sector of the economy [22].

In this regard, the importance of goats must be considered, since although it is important for the socioeconomic development of the study area, it is also important in the overgrazing process. This fact provokes that the canopy cannot regenerate in time, and therefore erosive processes dominate the system [23].

A study conducted in 2006 [24] used remote-sensing methods to examine local desertification processes in the Southeast Iberian Peninsula. In this current study, the authors present a different method for evaluating and mapping the impact of grazing around watering points. The main objective of the study was to investigate changes in vegetation and soil patterns in the drylands of the Southeast Iberian Peninsula over time, in relation to socio-economic changes. The study had four specific goals: (1) to analyze the spatial structure of imagery from two desert sites during three different time periods (mid-late 2000s, around 2015, and 2020) using semi-variograms; (2) to apply

Preprints (www.preprints.org) | NOT PEER-REVIEWED | Posted: 12 June 2023 doi:10.20944/preprints202306.0781.v1

the kriging interpolation technique to smooth brightness index values extracted from satellite images with a spatial resolution of 30-80 meters, in order to assess spatial and temporal land-cover patterns; (3) to use kriging prediction maps for change detection analysis to determine the direction and intensity of changes between study periods; and (4) to relate these findings to the socio-economic situation before and after the EU economic crisis, which affected grazing intensity and therefore the land-use and land-cover state of the study sites.

2. Study Area

The region under investigation is situated in the southeastern part of Spain, in the Almeria province, as shown in Figure 1. It spans approximately 50 square kilometers and includes Tabernas, the largest town in the area with a population of 4025 people. The nearest large urban center is the city of Almeria, which has a population of 199237 and is located 37 km to the south of Tabernas.

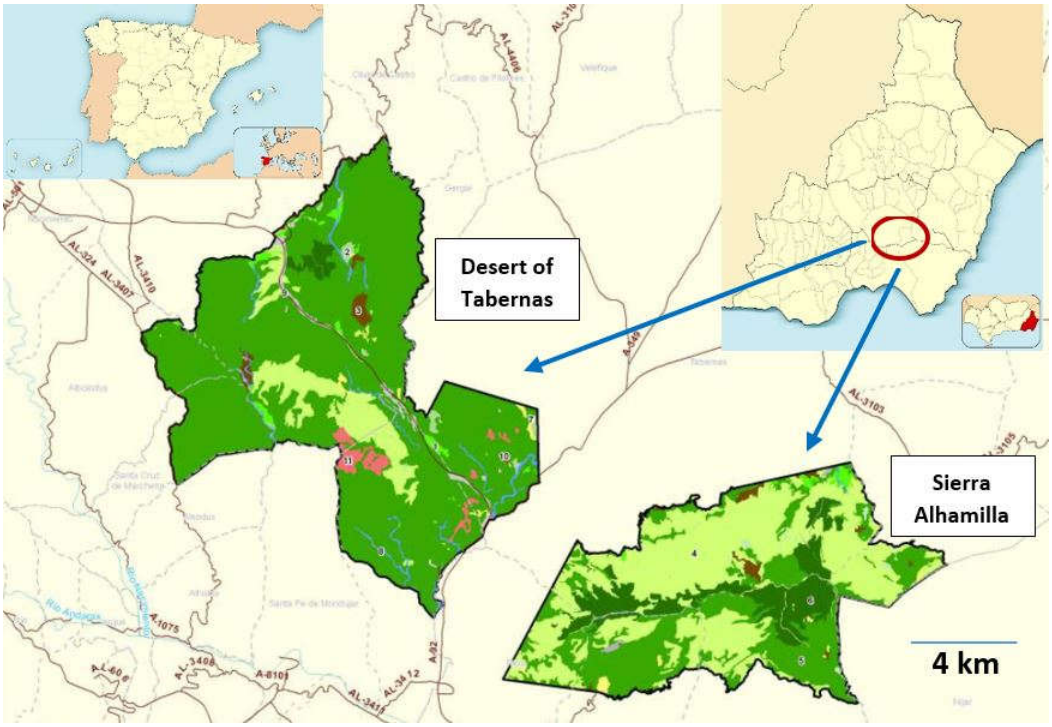

Figure 1. Location of the study area (Desert of Tabernas "37º 00′ 00′′ N; 02º 27′ 00′′ W" and Sierra Alhamilla "36º 59′ 20′′ N; 02º 21′ 05′′ W").

The central region of the study area, where human activities are concentrated, is the Tabernas valley. It is surrounded by two mountain ranges running from east to west: the Sierra de los Filabres to the north, and the Sierra Alhamilla to the south. In the western portion of the study area lies the Desert of Tabernas, which is regarded as the sole authentic desert in Europe meeting the desert criteria. Protection has been granted to both the Desert of Tabernas and a section of the Sierra Alhamilla as natural reserves [25].

The prevailing land cover types found in the region include vegetation consisting of bushes and grass, with or without trees [26]. Agriculture, primarily barley and some irrigated crops, is the primary land use, although it faces significant constraints due to the area's climatic and topographical conditions [27]. Nonetheless, within the past ten years, irrigated olive and almond plantations have been implemented. Currently, mining only occurs in a handful of gypsum quarries, and abandoned mines are prevalent in the area. While industry is not a major contributor to the local economy, the movie and entertainment industry has attracted numerous visitors in recent years. As a matter of fact, tourism is becoming increasingly important and could emerge as one of the primary economic activities in the future.

In another vein, according to Andalusian Government [28], in the study area the primary use is very scarce. This fact makes it possible for livestock activity to concentrate in areas where the canopy

 doi:10.20944/preprints202306.0781.v1

has reached a higher level of growth. It is evident that overgrazing, as well as livestock trampling, along with seasonal variation in rainfall regimes, leads to a progressive loss of existing vegetation, and as a result, a progressive loss of soil.

In reference to the loss of sustainability of the study area, it is of great interest to highlight the difference between the erosive and desertification processes that occur. According to Andalusian Government [28], the concept of desertification is more functional, starting to be considered as a disturbance that occurs in arid climates and that leads the system (human beings - natural resources) to an irreversible loss of sustainability. On the other hand, erosion consists of the loss of soil by uprooting, transport and subsequent accumulation, either by the action of wind or water. This process can be understood as a form of soil resource degradation, and therefore, an effect or symptom of desertification, but although it is not the only one. In this regard, and as is well known, although on a world scale the main form of erosion associated with desertification is wind, in the Iberian Peninsula water erosion predominates, constituting an endemic environmental problem in most of Mediterranean Spain. and, in particular, of the peninsular southeast (Desert of Tabernas and Sierra Alhamilla).

Regarding the climate of the study area, it should be noted, according to the Köppen and Geiger classification, that it is of the BSk type (local steppe).

The main climatic feature of the study area is its Mediterranean character, with mild temperatures and marked aridity. This is because the Betic mountains intersect the Atlantic fronts and leave this area in a rain shadow. The average annual precipitation is 239 mm and the number of rainy days per year ranges from 25 to 55, although only 6% of the rainy episodes exceed 20 mm. The average annual temperature is 17.9°C, the average minimum of the coldest month is between 3ºC and 10ºC, with the maximum exceeding 40°C in summer (sometimes reaching 48).

As is known, the study area is made up of loose sediments [29], highly salinized and easily washed away by rainwater. This fact, along with the sparse vegetation (Figure 2c) and torrential rains, caused the soil in these areas to erode almost completely (Figure 2b and e), excavating large gullies and ravines separated by steep slopes. On these slopes, erosion is intense and allows few plant species to take root, which is why they are often bare and give the landscape as a whole the characteristic desert appearance (Figure 2a, b, d and e).

Preprints (www.preprints.org) | NOT PEER-REVIEWED | Posted: 12 June 2023 doi:10.20944/preprints202306.0781.v1

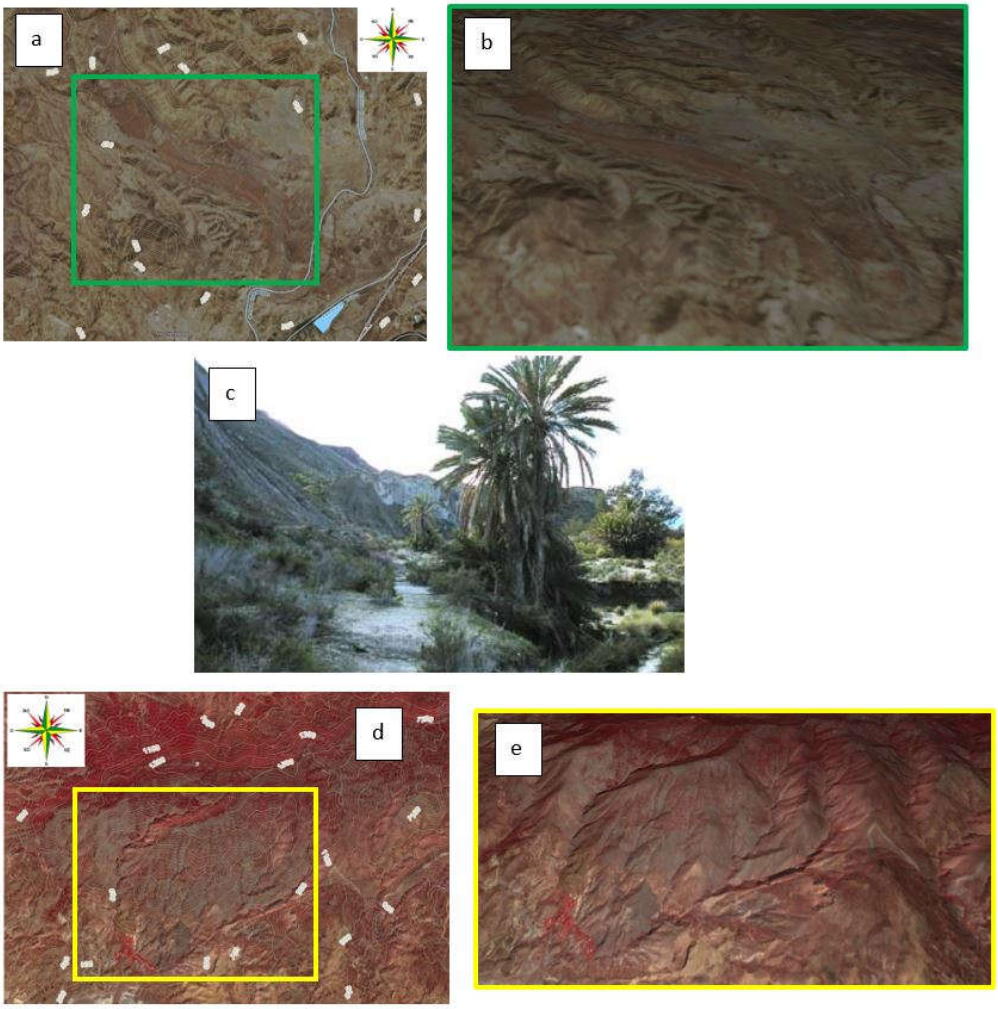

Figure 2. Desert of Tabernas in Sentinel-2 L2A RGB bands (432) combination (a and b). Sierra Alhamilla in Sentinel-2 L2A False color bands (843) combination (d and e). Typical vegetation (c) of the study area.

3. Materials and Methods

A total of 528 Landsat pictures were obtained from the Earth Explorer platform (https://earthexplorer.usgs.gov/) and utilized to cover the two research locations. These images were captured by the Thematic Mapper (TM) sensor of the Landsat 5 and Landsat 8 satellites at three different time intervals, as indicated in Table 1. The only land-use method in these areas is livestock grazing.

Table 1. Satellite images used in this study (both in the desert of Tabernas and in the Sierra Alhamilla).

Satellite and sensor	Nº of images	Date	Path/row (WRS-2)
Landsat 5 TM	188	Mid-late 2000s (January 1st, 2005 – December 31th, 2010)	199 and 200/034
Landsat 8 LC	204	Around 2015 (January 1st, 2014 – December 31th, 2016)	199 and 200/034
Landsat 8 LC	136	2020 (January 1st, 2019 – 31th, 2020)	199 and 200/034

The process of image processing commenced by transforming the digital numbers of the image into reflectance values [30-31]. From these values, various vegetation indices such as NDVI [32], SAVI [33], MSAVI [34], perpendicular vegetation index or PVI [35], and greenness and brightness indices [36] derived from tasseled cap were computed for each image subset. To determine the most

Preprints (www.preprints.org) | NOT PEER-REVIEWED | Posted: 12 June 2023 doi:10.20944/preprints202306.0781.v1

appropriate index for distinguishing degraded and non-degraded land, spectral separability analysis was carried out using the mean and standard deviation values of extreme classes in each scene, for all the indices [37-39]. The results of this analysis showed that the brightness index (BI) had the highest separability value, and hence, it was selected for further analysis (see Eq. 1).

$$BI = \sum_{i=1}^{n} \alpha_i \cdot B_i \quad (1)$$

According to [36-37], BI can be inferred for different sensors using spectral band numbers (B_i) and appropriate BI coefficients (α_i). One of the benefits of using the BI index is its ability to compare different sensors that have different spectral bands. This is possible because the BI values can be normalized to create a single layer of data, making comparisons between sensors possible. Further, the BI index was originally designed to analyze soil properties, and there have been statistically significant results using this method.

The following process involved averaging each window of 6 x 6 pixels in the TM (Landsat 5) and LC (Landsat 8) images, which reduced the resolution by a factor of 6. This resulted in a new pixel size of 171 meters, which was small enough to assess changes within the 6 km range from the watering point where degradation is expected. The subset size was reduced from around 1.5 million pixels to only 40000 pixels, which made the data more manageable for processing. Note that even though the pixel size was reduced, image-to-image geometric correction was applied for better accuracy in the change detection process.

In another vein, the geostatistics is based on the concept of a regionalized variable, which is a variable that can be characterized based on a number of spatial measurements. The fundamental idea behind geostatistics is that when spatial continuity is assumed, adjacent samples are expected to be more similar to each other than samples that are further apart. This spatial dependence can be statistically analyzed and described using parameters derived from a semi-variogram, which is a function that relates the semi-variance to the distance and direction between two samples. The semi-variance, defined as half the mean-squared difference between two samples that are a certain distance apart in a given direction, is used to quantify this spatial dependence. This approach provides a way to analyze and understand the spatial variation in a given variable (Eq. 2).

$$\gamma(h) = \frac{1}{2 \cdot N(h)} \cdot \sum_{i=1}^{N(h)} (Z_{xi} - Z_{xi+h})^2 \quad (2)$$

As is well known, the Eq. (2) referred to earlier uses a vector h to define both the direction and distance between two samples, which is commonly known as the lag.

In Eq. (2), the semi-variance at lag h is denoted by $\gamma(h)$, and $N(h)$ represents the number of pairs of samples that are separated by a distance of h. The value of the regionalized variable at a given location i is represented by Z_i. In addition to the lag, the variogram is characterized by three other parameters: the nugget, range, and sill. The nugget accounts for variability at zero distance and is attributable to errors in both sampling and analysis. The range represents the distance, often denoted as "a" beyond which spatial autocorrelation between sampling sites becomes negligible. The sill represents the variability of samples that are spatially independent. Empirical semi-variograms can be computed from a set of observations, and then a theoretical model can be fitted [40]. The exponential model is a popular theoretical model and is expressed in the form shown in Eq. (3), where C_0 is the nugget, $C_0 + C_1$ is the sill, a is the range and h is the lag.

$$\gamma(h) = C_0 + C_1 \cdot [1 - e^{(\frac{-3 \cdot |h|}{a})}] \quad (3)$$

To better understand the spatial structure of imagery for a given date and location, variogram analysis was used in the studied sites. The decision to use semi-variograms was based on the similarity in spatial structure of most of the variables, which gradually increased or decreased as the distance from the watering point increased, until grazing effects were no longer observed. Semi-variograms were introduced to remote sensing by [41], who found that variogram parameters could be directly linked to image features. In this study, the presence or absence of a sill in the variogram could indicate the presence of a radial grazing pattern around watering points, while the level of the

Preprints (www.preprints.org) | NOT PEER-REVIEWED | Posted: 12 June 2023 doi:10.20944/preprints202306.0781.v1

sill could be used to assess the homogeneity (i.e., lower variance) of an area. The lag distance in the variogram could also be related to the walking distance of livestock, with observations becoming increasingly independent beyond a certain distance (the range).

In each subset of the data, the empirical semi-variogram was calculated using 40000 pixels, and a theoretical model that best fit the semi-variogram was estimated. The model parameters were then determined by minimizing the squared differences between the empirical semi-variogram values and those of the theoretical model. Once the best-fitting model was chosen, several criteria were applied to assess its accuracy and to fine-tune its parameters: 1) it was carried out a cross-validation scatter plot; 2) it was inferred the mean estimation error using the Eq. (4); and 3) it was obtained the mean standardized squared estimation error through Eq. (5).

$$\frac{1}{n} \cdot \sum_{i=1}^{n} (Z_{xi} - Z_{xi}^{*}) = \frac{1}{n} \cdot \sum_{i=1}^{n} \varepsilon_i \approx 0 \tag{4}$$

$$\frac{1}{n} \cdot \sum_{i=1}^{n} [\frac{Z_{xi} - Z_{xi}^{*}}{S_i^{*}}]^2 = \frac{1}{n} \cdot \sum_{i=1}^{n} (\frac{\varepsilon_i}{S_i})^2 \approx 1 \tag{5}$$

In order to minimize the influence of local effects and obtain a more even representation of surface brightness values across the study sites, researchers employed a linear geostatistical method called ordinary kriging interpolation. This method, according to [42], is useful in revealing spatial phenomena. The approach estimates the mean of the values within a searching neighborhood as a constant.

The study employed the BI differencing method as a post-processing change detection technique, which is a modified version of the vegetation index differencing method [43]. Its purpose was to evaluate the primary patterns of degradation (in magenta color) or rehabilitation (in green color) in the study areas. To achieve this, two sets of kriging maps (i.e., 2016-2005 and 2020-2016) were subtracted for each site (desert of Tabernas and Sierra Alhamilla).

4. Results and Discussion

Figure 3 displays the relevant BI products, which were computed using Eq. (1) and the corresponding coefficients. The bright areas that are scattered across the mid to late 2000s images, indicating watering areas, are much less visible in the 2015 and 2020 images. In the more recent 2020 image of the desert of Tabernas and Sierra Alhamilla, many watering areas are absent, but there is a large bright area present. The brightness index (BI) values, which indicate bare, degraded soil, were calculated using the same method for all sensors, and the brightness levels were uniformly stretched. The desert of Tabernas has BI values ranging from 0.66 to 0.95, while the Sierra Alhamilla sites have BI values ranging from 0.20 to 0.60.

The geostatistical analysis utilized all of the BI images. Initially, empirical semi-variograms were created for each of the two sites for the three time periods. Field observations did not reveal any anisotropic patterns that could potentially govern the direction of grazing, such as linear dunes or other barriers. Therefore, an isotropic distribution was assumed in all cases. The results of the cross-validation analyses are outlined in Table 2. The slope coefficient and the intercept coefficient of the exponential model chosen were very close to unity and zero, respectively, indicating that the model was able to accurately replicate the observed values.

Following the examination of several theoretical models [40], the exponential model (Eq. 3) was chosen as it yielded the best results during cross-validation. The fit of the model was assessed using the least-squares measure, and the variogram parameters can be found in Table 2. Each variogram was processed with 17 lags, each spanning a distance of 800 m. The lag values were determined through a trial and error process to optimize the aforementioned criteria. When observed visually, the variograms from the mid-late 2000s and around 2015 appear quite similar, exhibiting a typical variogram shape. Two notable features can be observed. Firstly, the sill of the variogram around 2015 is lower compared to the mid-late 2000s, suggesting a decrease in variance in the latter year. Further, the range in the mid-late 2000s is 4800 m, while in around 2015 it is 6400 m, which corresponds to the

Preprints (www.preprints.org) | NOT PEER-REVIEWED | Posted: 12 June 2023 doi:10.20944/preprints202306.0781.v1

reported walking distance of livestock from their drinking source [44]. In contrast, the variogram for 2020 only reaches a similar sill level after a distance of 12 km. This range does not appear to be indicative of the grazing pattern in the region.

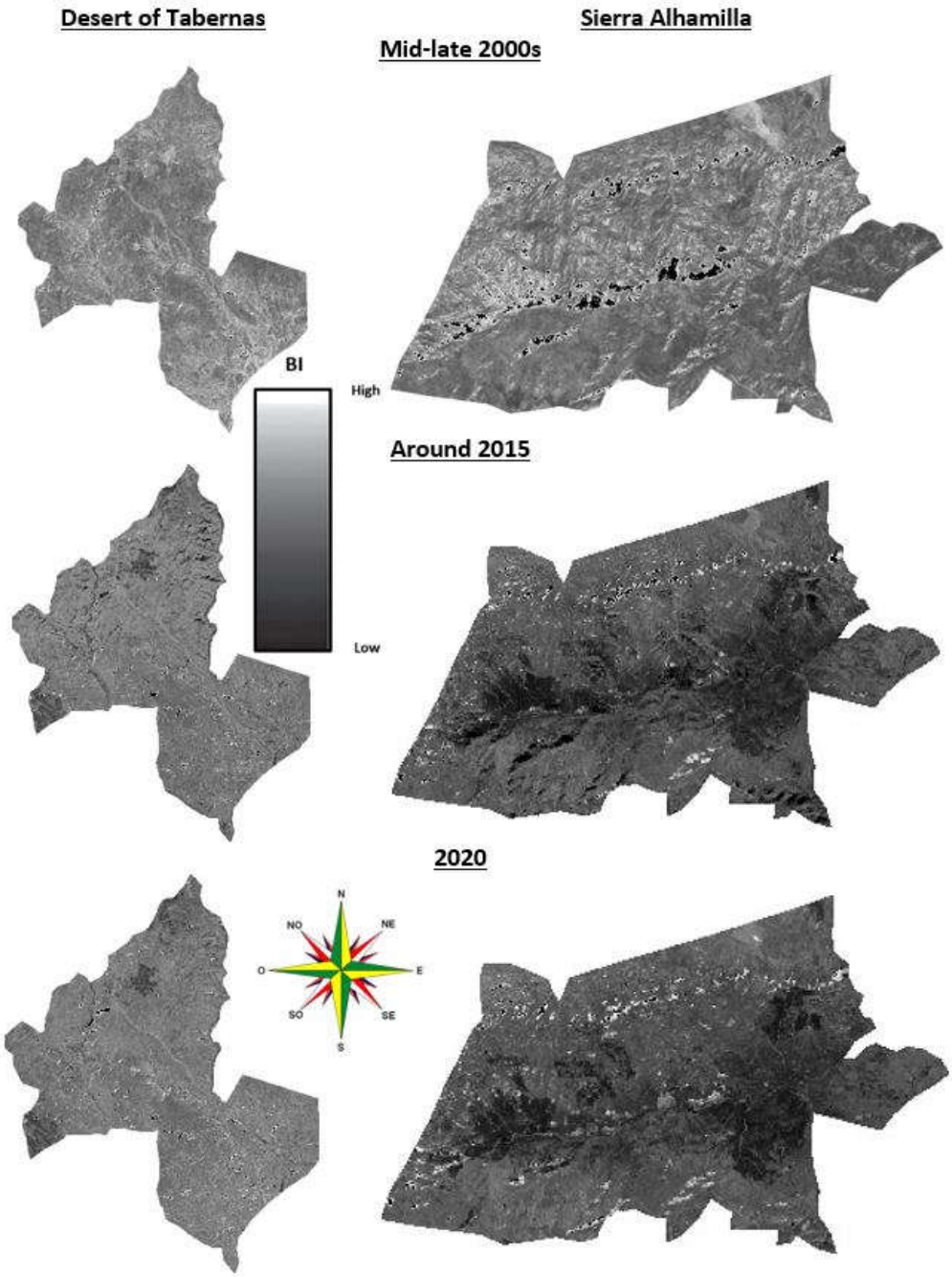

Figure 3. Brightness index (BI) in the study area at different date. All images of each study area, corresponding to a determined period of time, are the images resulting from the treatment carried out with all the images of each period.

Table 2. Variogram parameters in the study area.

Study area	Date	Nugget	Sill	Range (m)	Spatial variance
Tabernas and Alhamilla	Mid-late 2000s	0	0.00088	4800	0.00088
	Around 2015	0.0001	0.00064	6400	0.00054
	2020	0.0001	0.0008	12000	0.0007

Preprints (www.preprints.org) | NOT PEER-REVIEWED | Posted: 12 June 2023 doi:10.20944/preprints202306.0781.v1

Later, kriging interpolation techniques were utilized, employing exponential models (see Figure 4) with parameters from Table 2. The final outcomes illustrating the distribution of BI values for the three periods and both sites are displayed in Figure 5. The initial maps, specifically during the mid-late 2000s, reveal the presence of bands encircling the watering points, signifying the progressive degradation of land extending from the wells. These bands denote the grazing gradient or the impact of grazing. Regions depicted in dark red in the images indicate areas where grazing impact predominates, exerting a strong influence on spatial variation. Such regions are referred to as the "sacrifice zone" by [11]. The adjacent belts in light red, orange and yellow represent a mixed zone where the effects of grazing and natural variability coincide or establish a stable balance. This zone can be likened to the outskirts of the grazing impact and highlights the primary migration routes of livestock. The zone exhibiting green shades signifies an area where natural variability surpasses the impact of grazing and is termed the "grazing reserve" by [11].

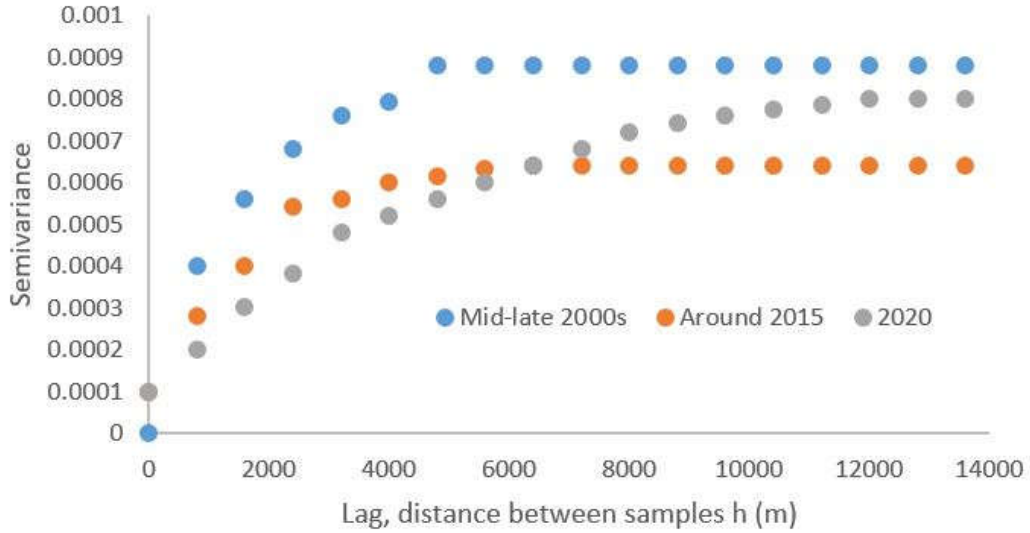

Figure 4. Model variograms obtained from Brightness Index (BI) in the Desert of Tabernas and Sierra Alhamilla.

The BI differencing method, explained in the concluding paragraph of Section 3, was utilized to analyze changes in grazing patterns over two specific time periods. Figure 6 displays the maps illustrating these changes. In the change detection map for the period 2016-2005, a large portion of the area appears grey, indicating that there were no noticeable alterations in grazing patterns. The remaining areas are represented by magenta, indicating degradation, and green tones, representing rehabilitation. Consequently, between the mid-late 2000s and around 2015, the overall trend was a positive one, with land-cover conditions improving or undergoing rehabilitation. It is worth noting that around 2015, the area became more uniform, as indicated by the reduced variation (lower sill) in Figure 4 and the narrower range of colors in Figure 6a and b. Conversely, during the second period (2020-2016), a significant portion of the area experienced degradation processes (magenta colors), while the area undergoing rehabilitation (green tones) diminished considerably (Figure 6a and b).

Preprints (www.preprints.org) | NOT PEER-REVIEWED | Posted: 12 June 2023 doi:10.20944/preprints202306.0781.v1

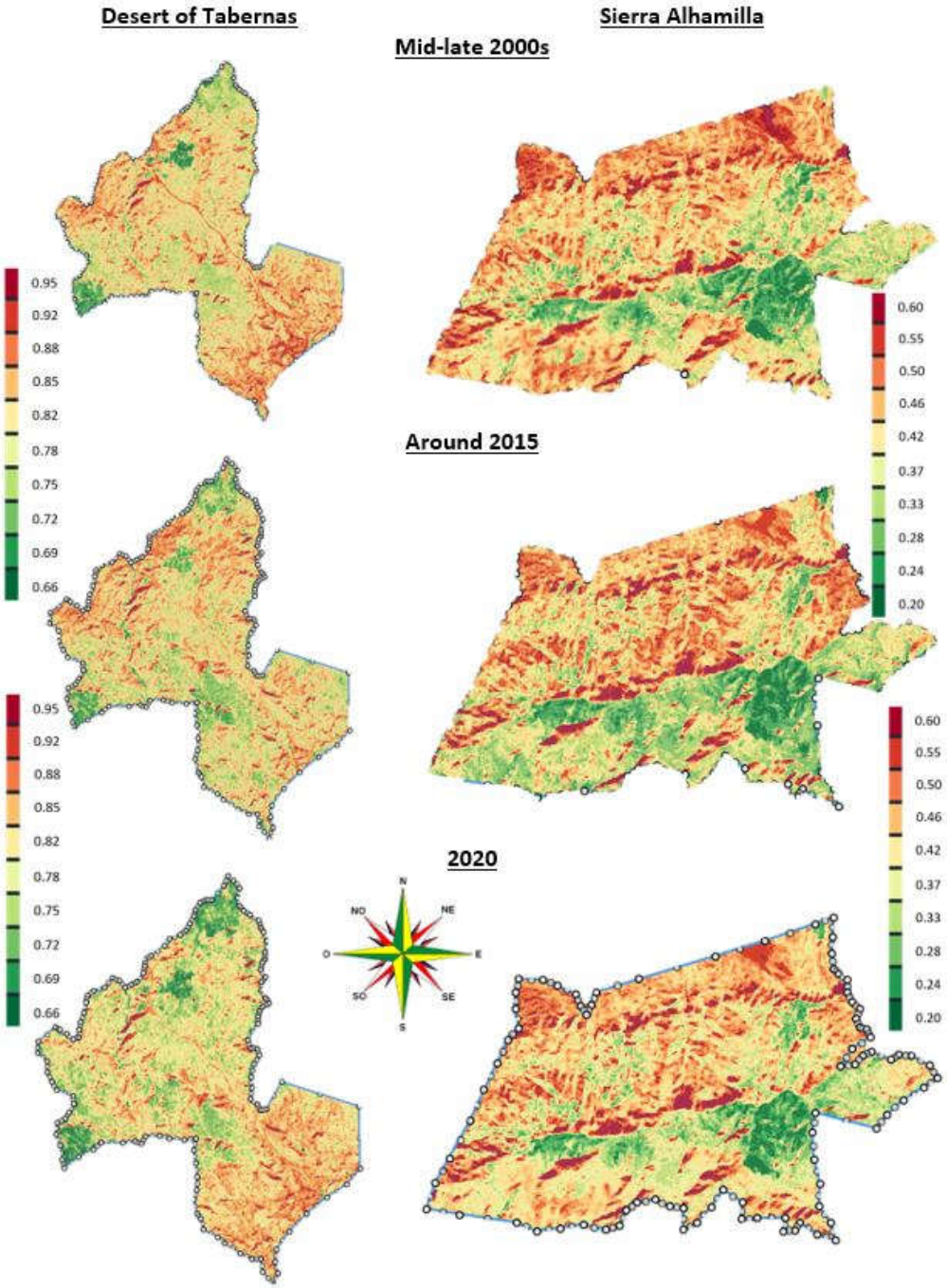

Figure 5. Kriging maps inferred by interpolation in the Desert of Tabernas and Sierra Alhamilla.

As a result of the 2007 economic crisis, there was a progressive decrease in the livestock census in the study area due to increased costs, which is why many farmers had to abandon economic activity due to lack of profitability. This fact had a positive influence on the environment, since it led to the recovery of those areas where livestock pressure was highest. This is one of the reasons why, from the mid-late 2000s to around 2015, a recovery of the study area can be observed (see Figure 6a). Despite the above, and although in 2016 the Andalusian Government started the Recovery Plan for the Desert of Tabernas and Sierra Alhamilla [45], the increase in degradation (Figure 6b) is mainly due to climatic causes.

Preprints (www.preprints.org) | NOT PEER-REVIEWED | Posted: 12 June 2023 doi:10.20944/preprints202306.0781.v1

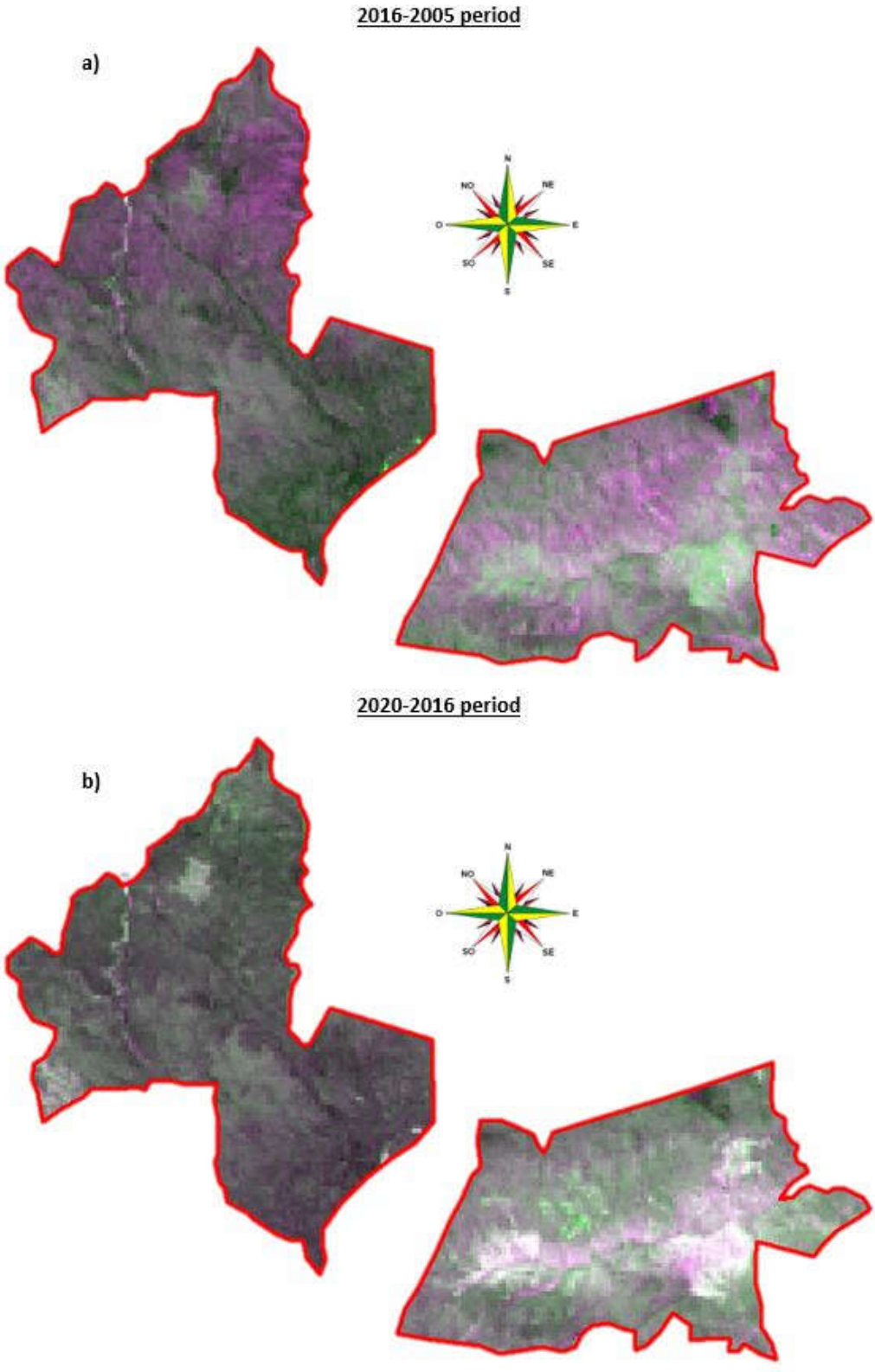

Figure 6. Result of the BI differencing method in the Desert of Tabernas (left side) and Sierra Alhamilla (right side) for both 2016-2005 (a) and 2020-2016 (b) periods.

To explain the climatic effect in the study area, Table 3 shows the data corresponding to the sum of both average monthly temperature (in Celsius) and monthly precipitation (in mm), in each of the years subjected to study. All climatic data were downloaded from Version 4 of the CRUTS monthly high-resolution gridded multivariate climate dataset [46].

Preprints (www.preprints.org) | NOT PEER-REVIEWED | Posted: 12 June 2023 doi:10.20944/preprints202306.0781.v1

Table 3. Climatic data in the study area from 2005 to 2020.

Year	Tª (ºC)	P (mm)	Year	Tª (ºC)	P (mm)
2005	179.6	226.6	2013	185.1	385.6
2006	180.7	392.3	2014	186.1	293.5
2007	182.2	410.8	2015	187.1	338.4
2008	183.7	407.3	2016	189.9	320.5
2009	185.0	428.2	2017	190.6	293.3
2010	185.3	646.6	2018	191.6	490.7
2011	184.2	333.0	2019	194.6	340.8
2012	184.8	386.1	2020	193.7	359.5

From Table 3, a new aridity index was obtained to help explain the results shown in Figure 6. Said index, which we have called the RAMALL (**RA**mírez, **MA**dueño, **L**ópez and **L**eiva) Aridity Index. Eq. (6) specifies how the RAMALL index is calculated.

$$RAMALL\ Aridity\ Index = \frac{\sum_{i=1}^{12} MP_j}{\sum_{i=1}^{12} AMT_j + \sum_{i=1}^{12} AMT_{j+1}} \quad (6)$$

where:
i = months of each year.
j = year in which you want to calculate RAMALL aridity index.
MP_j = monthly precipitation (mm) in the year "j".
AMT_j = average monthly temperature (ºC) in the year "j".
AMT_{j+1} = average monthly temperature (ºC) in the year "j+1".

Values greater than 1 indicate low aridity index, while values lower than 1 indicate low aridity index. Figure 7 shows the evolution of this new RAMALL aridity index in the study area between 2005 and 2020.

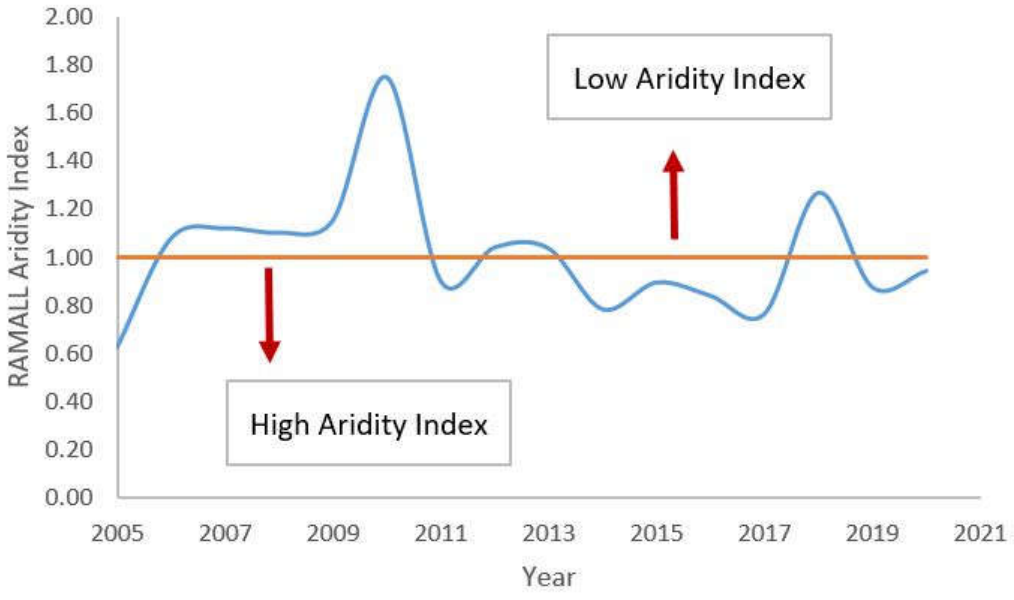

Figure 7. RAMALL aridity index during the study period in the Desert of Tabernas and Sierra Alhamilla ($\sum AMT_{2021}$ = 186.51 ºC).

After analyzing the data shown in Table 3, as well as Figure 7, the RAMALL aridity index presents mean values of 1.05 (low aridity index) between 2005 and 2015, and 0.94 (high aridity index) between 2016 and 2020.

Preprints (www.preprints.org) | NOT PEER-REVIEWED | Posted: 12 June 2023 doi:10.20944/preprints202306.0781.v1

As can be seen, the 2007 economic crisis had a positive effect on the average aridity during the 2016-2005 period (RAMALL aridity index value greater than 1). During this period, the water erosion phenomena [28] were minimized not only by the decrease in livestock pressure, but also as a consequence of the increase in plant variety that, being present in the soil seed bank, only colonized the area study as a result of said decreased grazing.

However, in the second period under study (2020-2016 period), whose RAMALL aridity index values are lower than 1, the progressive increase in the average annual temperature (Figure 8), along with the almost disappearance of grazing that occurred at the end of the first period (2016-2005), favored the plant variety loss in the study area, and therefore the shrub stratum was dominant. This fact has, as a serious consequence for the environment of the study area, an increase in erosive processes, as well as both the soil and habitat loss over time if the global warming trend continues [28].

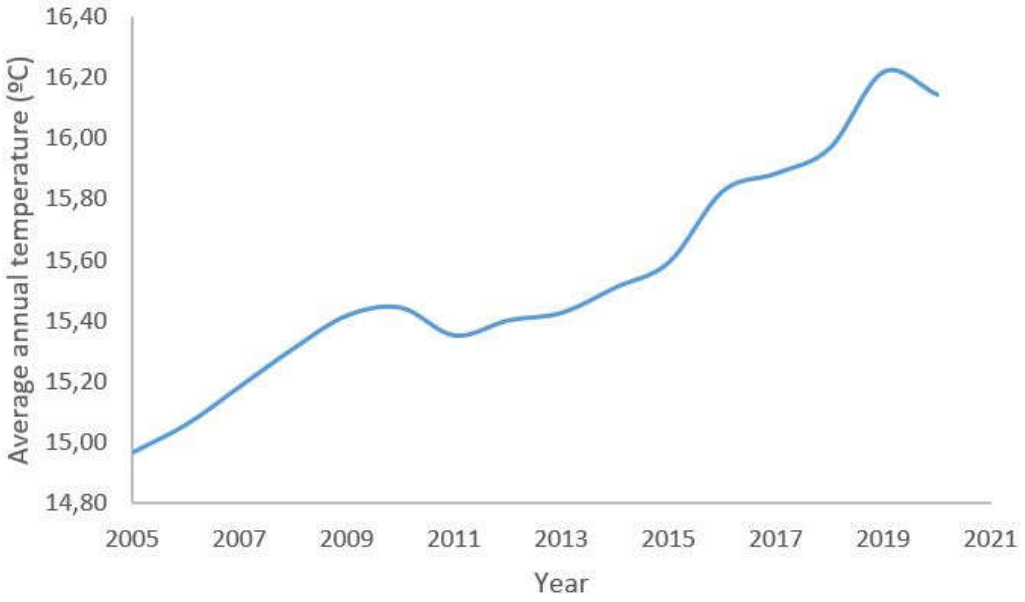

Figure 8. Average annual temperature evolution in the study area between 2005 and 2020.

Finally, it is necessary to emphasize that, both in the desert of Tabernas and Sierra Alhamilla, the influence of the arid climate has given rise, over time, to a landscape of mainly erosive morphology, whose main signs are the slopes (of soft materials) in the form of gullies. With respect to the drainage network, it is necessary to indicate the action of the existing channels on the smoothing of the relief, resulting in a predominance of erosive action at the headwaters, and therefore, the boxing in of the channels, as well as a predominance of sedimentation in its lower part. The impact caused by raindrops on bare soil gives rise to a wide variety of microforms in the landscape, a key characteristic of soil loss through surface runoff.

5. Conclusions

The aim of the present study was to analyze the changes in vegetation patterns over time in the desert of Tabernas and Sierra Alhamilla (Almería, Spain), focusing on land degradation and rehabilitation. Specifically, the research aimed to understand how these changes were influenced by socio-economic factors following the economic crisis in 2007. To achieve this, the tasseled cap-derived brightness index (BI) was employed as a tool to depict the spatial distribution of land surface characteristics. The BI was chosen for its superior ability to differentiate among various spectral indices, its original purpose of examining soil properties, and its capability to compare different sensors with distinct spectral bands by normalizing them into a single BI layer.

The use of geostatistical analysis, specifically semi-variance analysis, was determined to be a suitable approach for understanding the spatial structure within imagery at a specific date and

location. This method was chosen due to the similarity between the variogram's shape and the directional changes observed in various biotic, abiotic, and environmental variables along the grazing gradient emanating from watering points in arid and semi-arid regions. By utilizing variogram models from the mid-late 2000s and around 2015, it becomes possible to quantitatively generalize the observed phenomena across the region of interest. The average range of 4800-6400 meters aligns with the reported walking distance of livestock from their water source. Comparing variograms from different years can provide insights into the temporal dynamics of the region, as evidenced by the failure to reach a sill in the variogram when grazing ceased at the end of 2015.

The kriging interpolation method was employed as a smoothing filter, whereby each pixel in the image was replaced with the solution derived from the variogram equation (specifically, an exponential model in this case) calculated using all other pixels. This approach aimed to reduce spatial errors and fine-scale variability, facilitating a more accurate delineation of degradation boundaries surrounding the watering points. The resulting maps of the study area revealed a radial pattern, indicating progressive land degradation emanating from the wells, commonly referred to as the grazing gradient. However, this pattern appeared blurred or absent in the 2020 maps. In comparison to other interpolation techniques, ordinary kriging is regarded as the superior linear unbiased estimator.

The index differencing technique was successfully utilized to analyze temporal changes. This study showcases the capability of satellite image analysis to track land-use and land-cover modifications resulting from both the 2007 economic crisis and the significant decrease in grazing pressure.

Author Contributions: Conceptualization, E.R.J., A.M.-L, J.M.M.L, M.C.L.G and J.L.L.P.; methodology, E.R.J., A.M.-L, J.M.M.L, M.C.L.G and J.L.L.P.; formal analysis, E.R.J., A.M.-L, J.M.M.L, M.C.L.G and J.L.L.P.; investigation, E.R.J., A.M.-L, J.M.M.L, M.C.L.G and J.L.L.P.; resources, E.R.J., A.M.-L, J.M.M.L, M.C.L.G and J.L.L.P.; writing—original draft preparation, E.R.J., A.M.-L, J.M.M.L, M.C.L.G and J.L.L.P.; writing—review and editing, E.R.J., A.M.-L, J.M.M.L, M.C.L.G and J.L.L.P.; supervision, E.R.J., A.M.-L, J.M.M.L, M.C.L.G and J.L.L.P.; project administration, E.R.J. All authors have read and agreed to the published version of the manuscript.

Funding This research received no external funding.

Data Availability Statement: The data used to support the findings of this study can be made available by the corresponding author upon request.

Acknowledgments: This study has been carried out thanks to the research project with Reference "OG-017/07". Authors are grateful for the disinterested collaboration of the Knowledge-Based Company RSV3 Remote Sensing S.L.

Conflicts of Interest: The authors declare no conflict of interests.

References

1. Lin, X.; Zhao, H.; Zhang, S.; Li, X.; Gao, W.; Ren, Z.; Luo, M. Effects of animal grazing on vegetation biomass and soil moisture on a typical steppe in Inner Mongolia, China. *Ecohydrology*. **2022**, 15(1), e2350. DOI: 10.1002/eco.2350
2. Chen, T.; Tang, G.; Yuan, Y.; Guo, H.; Xu, Z.; Jiang, G.; Chen, X. Unraveling the relative impacts of climate change and human activities on grassland productivity in Central Asia over last three decades. *Science of the Total Environment*. **2020**, 743, 140649. DOI: 10.1016/j.scitotenv.2020.140649
3. Hamidov, A.; Helming, K.; Balla, D. Impact of agricultural land use in Central Asia: a review. *Agronomy for sustainable development*. **2016**, 36, 6–23. DOI: 10.1007/s13593-015-0337-7
4. Augusteyn, J.; Rich, M.; Mitchell, C.; Mulder, E.; Nolan, B.; Lim, L.; Melzer, R. Does reducing grazing pressure or predation conserve kowaris? A case study at Diamantina National Park. *Australian Journal of Zoology*. **2022**, 70(2), 56-73. DOI: 10.1071/ZO22027
5. Yang, X.; Zhang, K.; Jia, B.; Ci, L. Desertification assessment in China: An overview. *Journal of Arid Environments*. **2005**, 63(2), 517-531. DOI: 10.1016/j.jaridenv.2005.03.032
6. Malan, J.A.C. Offstream watering points for cattle as a method for riparian restoration, Ph. D. Dissertation. Central Queensland University, Queensland, Australia. 2020. DOI: 10.25946/14274524.v1
7. Fokeng, R.M.; Fogwe, Z.N. Landsat NDVI-based vegetation degradation dynamics and its response to rainfall variability and anthropogenic stressors in Southern Bui Plateau, Cameroon. *Geosystems and Geoenvironment*. **2022**, 1(3), 100075. DOI: 10.1016/j.geogeo.2022.100075

8. Bakhshi, J.; Javadi, S.A.; Tavili, A.; Arzani, H. Study on the effects of different levels of grazing and exclosure on vegetation and soil properties in semi-arid rangelands of Iran. *Acta Ecologica Sinica*. **2020**, 40(6), 425-431. DOI: 10.1016/j.chnaes.2019.07.003
9. Ahlborn, J.; von Wehrden, H.; Lang, B.; Römermann, C.; Oyunbileg, M.; Oyuntsetseg, B.; Wesche, K. Climate–grazing interactions in Mongolian rangelands: Effects of grazing change along a large-scale environmental gradient. *Journal of Arid Environments*. **2020**, 173, 104043. DOI: 10.1016/j.jaridenv.2019.104043
10. Ma, L.; Derner, J.D.; Harmel, R.D.; Tatarko, J.; Moore, A.D.; Rotz, C.A; ...; Wilmer, H. Application of grazing land models in ecosystem management: Current status and next frontiers. *Advances in Agronomy*. **2019**, 158, 173-215. DOI: 10.1016/bs.agron.2019.07.003
11. Van der Weyde, L.K.; Theisinger, O.; Mbisana, C.; Gielen, M.C.; Klein, R. The value of pastoral ranches for wildlife conservation in the Kalahari. *Wildlife Research*. **2021**, 49(3), 215-226. DOI: 10.1071/WR21048
12. Henriques, M.; McVicar, T.R.; Holland, K.L.; Daly, E. Riparian vegetation and geomorphological interactions in anabranching rivers: A global review. *Ecohydrology*. **2022**, 15(2), e2370. DOI: 10.1002/eco.2370
13. Donohue, R.J.; Mokany, K.; McVicar, T.R.; O'Grady, A.P. Identifying management-driven dynamics in vegetation cover: Applying the Compere framework to Cooper Creek, Australia. *Ecosphere*. **2022**, 13(3), e4006. DOI: 10.1002/ecs2.4006
14. Rivera-Marin, D.; Dash, J.; Ogutu, B. The use of remote sensing for desertification studies: A review. *Journal of Arid Environments*. **2022**, 206, 104829. DOI: 10.1016/j.jaridenv.2022.104829
15. Wang, G.; Li, J.; Ravi, S. A combined grazing and fire management may reverse woody shrub encroachment in desert grasslands. *Landscape Ecology*. **2019**, 34, 2017-2031. DOI: 10.1007/s10980-019-00873-0
16. El Aich, A.; Pueyo, Y.; Barrantes Díaz, O.; Alados Lopez, C. Management and restoration of pastures and rangelands in the Mediterranean basin from the Northern and the Southern perspective. *Options Méditerranéennes*. **2021**; 125, 257-270.
17. Dara, A.; Baumann, M.; Freitag, M.; Hölzel, N.; Hostert, P.; Kamp, J.; ...; Kuemmerle, T. Annual Landsat time series reveal post-Soviet changes in grazing pressure. *Remote Sensing of Environment*. **2020**, 239, 111667. DOI: 10.1016/j.rse.2020.111667
18. Ganem, K.A.; Xue, Y.; Rodrigues, A.D.A.; Franca-Rocha, W.; Oliveira, M.T.D.; Carvalho, N.S.D.; ...; Shimabukuro, Y.E. Mapping South America's Drylands through Remote Sensing—A Review of the Methodological Trends and Current Challenges. *Remote Sensing*. **2022**, 14(3), 736. DOI: 10.3390/rs14030736
19. Li, C.; de Jong, R.; Schmid, B.; Wulf, H.; Schaepman, M.E.. Spatial variation of human influences on grassland biomass on the Qinghai-Tibetan plateau. *Science of the Total Environment*. **2019**, 665, 678-689. DOI: 10.1016/j.scitotenv.2019.01.321
20. Nyamuryekung'e, S.; Cibils, A.F.; Estell, R.E.; VanLeeuwen, D.; Spiegal, S.; Steele, C.; ...; Cao, H. Movement, activity, and landscape use patterns of heritage and commercial beef cows grazing Chihuahuan Desert rangeland. *Journal of Arid Environments*. **2022**, 199, 104704. DOI: 10.1016/j.jaridenv.2021.104704
21. Asmare, B. A review of sensor technologies applicable for domestic livestock production and health management. *Advances in Agriculture*. **2022**, 1-6. DOI: 10.1155/2022/1599190
22. Giménez-Anaya, A.; Bueno, C.G.; Fernández-Llario, P.; Fonseca, C.; García-González, R.; Herrero, J.; ...; Rosell, C. What Do We Know About Wild Boar in Iberia?. In *Problematic Wildlife II*, 1st ed.; Angelici, F., Rossi, L., Eds.; Springer: Cham, Switzerland, 2020; Volume 2, pp. 251-271. DOI: 10.1007/978-3-030-42335-3_9
23. Lozano Cantero, F.J. Informe sobre el desierto de Tabernas. Diputación Provincial de Almería. **2006**, 50 pp. Available online: http://www.almeria.es/Servicios/Informacion/Informacion.nsf/aff1dd050488813ac1256ae10033dfd3/5d0fdfb5dc132372c1257384004d0958/$FILE/Estudio.pdf (Accessed on 15 March 2023).
24. Alemayehu, T.; Recatalá, L.; Fabbri, A. G.; Sánchez, J. Land use change detection as a basis for analysing desertification processes: A case study in Tabernas (Almeria, Spain). In *Desertification in the Mediterranean Region. A Security Issue*, 1st ed.; Kepner, W.G., Rubio, J.L., Mouat, D.A., Pedrazzini, F., Eds.; Springer: Netherlands, 2006; Volume 1, pp. 341-352. DOI: 10.1007/1-4020-3760-0_15
25. Andalusian Government. Decreto 172/2016, de 8 de noviembre, por el que se declaran las Zonas Especiales de Conservación de la Red Ecológica Europea Natura 2000. **2016**. Available online: https://www.juntadeandalucia.es/medioambiente/portal/landing-page-normativa/-/asset_publisher/5WqqWSjN2vgc/content/decreto-172-2016-de-8-de-noviembre-por-el-que-se-declaran-las-zonas-especiales-de-conservaci-c3-b3n-de-la-red-ecol-c3-b3gica-europea-natura-2000-karst/20151. (Accessed on 15 March 2023).
26. Verhoeven, V.B.; Dedoussi, I.C. Annual satellite-based NDVI-derived land cover of Europe for 2001–2019. *Journal of Environmental management*. **2022**, 302, 113917. DOI: 10.1016/j.jenvman.2021.113917
27. Lázaro, R.; Calvo-Cases, A.; Rodriguez-Caballero, E.; Arnau-Rosalén, E.; Alexander, R.; Rubio, C.; ...; Puigdefábregas, J. Biocrusts and catchment asymmetry in Tabernas Desert (Almeria, Spain). *Geoderma*. **2022**, 406, 115526. DOI: 10.1016/j.geoderma.2021.115526
28. Andalusian Government. Valores ambientales de la zona de especial conservación Desierto de Tabernas (ES0000047). **2016**. Available online:

https://www.juntadeandalucia.es/medioambiente/portal_web/web/temas_ambientales/espacios_protegidos/01_renpa/canales_figuras_proteccion/Red_Natura/2016_06_valores_ambientales_resumenes/nuevos/0000047_desierto_tabernas.pdf (Accessed on 15 March 2023).

29. Veneranda, M.; Lopez-Reyes, G.; Manrique-Martinez, J.A.; Sanz-Arranz, A.; Medina, J.; Pérez, C., ...; Rull, F. Raman spectroscopy and planetary exploration: Testing the ExoMars/RLS system at the Tabernas Desert (Spain). *Microchemical Journal*. **2021**, 165, 106149. DOI: 10.1016/j.microc.2021.106149
30. Bannari, A.; Al-Ali, Z.M. Assessing climate change impact on soil salinity dynamics between 1987–2017 in arid landscape using Landsat TM, ETM+ and OLI data. *Remote Sensing*. **2020**, 12(17), 2794. DOI: 10.3390/rs12172794
31. ED Chaves, M.; CA Picoli, M.; D. Sanches, I. Recent applications of Landsat 8/OLI and Sentinel-2/MSI for land use and land cover mapping: A systematic review. *Remote Sensing*. **2020**, 12(18), 3062. DOI: 10.3390/rs12183062
32. Tucker, C.J. Red and photographic infrared linear combinations for monitoring vegetation. *Remote Sensing of Environment*. **1979**, 8(2), 127-150. DOI: 10.1016/0034-4257(79)90013-0
33. Huete, A.R. A soil-adjusted vegetation index (SAVI). *Remote Sensing of Environment*. **1988**, 25(3), 295-309. DOI: 10.1016/0034-4257(88)90106-X
34. Qi, J.; Chehbouni, A.; Huete, A.R.; Kerr, Y.H.; Sorooshian, S. A modified soil adjusted vegetation index. *Remote sensing of environment*. **1994**, 48(2), 119-126. DOI: 10.1016/0034-4257(94)90134-1
35. Richardson, A.J.; Wiegand, C.L. Distinguishing vegetation from soil background information. *Photogrammetric engineering and remote sensing*. **1977**, 43(12), 1541-1552.
36. Kauth, J.; Thomas, G.S. The tasseled cap—a graphic description of the spectral-temporal development of agricultural crops as seen by LANDSAT. In: Proceedings of the Symposium on Machine Processing of Remotely Sensed Data. Purdue University of West Lafayette, Indiana, EEUU, 1976 (01 01 1976).
37. Remer, L.A.; Levy, R.C.; Mattoo, S.; Tanré, D.; Gupta, P.; Shi, Y.; ...; Holben, B.N. The dark target algorithm for observing the global aerosol system: Past, present, and future. *Remote sensing*. **2020**, 12(18), 2900. DOI: 10.3390/rs12182900
38. Llorens, R.; Sobrino, J.A.; Fernández, C.; Fernández-Alonso, J.M.; Vega, J.A. A methodology to estimate forest fires burned areas and burn severity degrees using Sentinel-2 data. Application to the October 2017 fires in the Iberian Peninsula. *International Journal of Applied Earth Observation and Geoinformation*. **2021**, 95, 102243. DOI: 10.1016/j.jag.2020.102243
39. Ramírez-Juidías, E.; Cabello-Franco, E.J. New Remote Sensing Technologies Applied to the Prediction of Spontaneous Forest Fires. In *Natural Hazards-New Insights*, 1st ed.; Mokhtari, M., Ed.; Publisher: IntechOpen, 2023. DOI: 10.5772/intechopen.110501
40. Lu, C.; Song, Z.; Wang, W.; Zhang, Y.; Si, H.; Liu, B.; Shu, L. Spatiotemporal variation and long-range correlation of groundwater depth in the Northeast China Plain and North China Plain from 2000~2019. *Journal of Hydrology: Regional Studies*. **2021**, 37, 100888. DOI: 10.1016/j.ejrh.2021.100888
41. Qiu, S.; Zhu, Z.; Olofsson, P.; Woodcock, C.E.; Jin, S. Evaluation of Landsat image compositing algorithms. *Remote Sensing of Environment*. **2023**, 285, 113375. DOI: 10.1016/j.rse.2022.113375
42. Ramírez-Juidías, E.; Amaro-Mellado, J.L.; Leiva-Piedra, J.L. Influence of the Urban Green Spaces of Seville (Spain) on Housing Prices through the Hedonic Assessment Methodology and Geospatial Analysis. *Sustainability*. **2022**, 14(24), 16613. DOI: 10.3390/su142416613
43. Goswami, A.; Sharma, D.; Mathuku, H.; Gangadharan, S.M.P.; Yadav, C.S.; Sahu, S.K.; ...; Imran, H. Change detection in remote sensing image data comparing algebraic and machine learning methods. *Electronics*. **2022**, 11(3), 431. DOI: 10.3390/electronics11030431
44. Cowley, R.; Walsh, D. Modelling pasture growth and utilization in a large multi-watered paddock, 1st ed.; Northern Territory Government: Australia, 2023; pp. 1-52.
45. Boletín Oficial de la Junta de Andalucía (BOJA). BOJA 245, Friday, December 23, 2016. Available online: https://www.juntadeandalucia.es/medioambiente/portal/documents/20151/808488/4_anexo9_porn_alhamilla_tabernas_boja.pdf/654776f2-3228-9901-f582-7485caf4a92c?t=1511693637000 (accessed on 10 May 2023).
46. Harris, I.; Osborn, T.J.; Jones, P.; Lister, D. Version 4 of the CRU TS monthly high-resolution gridded multivariate climate dataset. *Scientific data*. **2020**, 7(1), 109. DOI: 10.1038/s41597-020-0453-3